Atomic-Scale Characterization of N-Doped Si Nanocrystals Embedded in SiO2 by Atom Probe Tomography

Rémi Demoulin, Manuel Roussel, Sébastien Duguay, Dominique Muller, Daniel Mathiot, Philippe Pareige, Etienne Talbot

Atomic-Scale Characterization of N-Doped Si Nanocrystals Embedded in SiO_2 by Atom Probe Tomography

Rémi Demoulin,[†] Manuel Roussel,[†] Sébastien Duguay,[†] Dominique Muller,[‡] Daniel Mathiot,[‡] Philippe Pareige,[†] and Etienne Talbot*[,†]

[†]Normandie Univ, UNIROUEN, INSA Rouen, CNRS, Groupe de Physique des Matériaux, 76000 Rouen, France

[‡]ICube Laboratory, Université de Strasbourg and CNRS, B.P. 20, 67037 Strasbourg Cedex, France

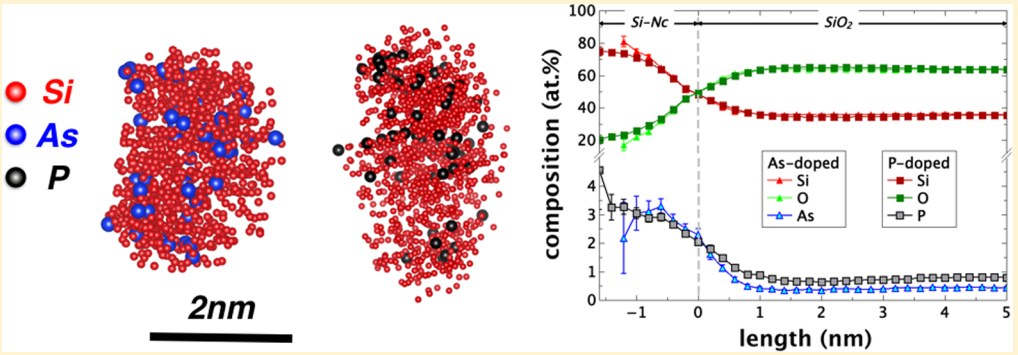

ABSTRACT: Structural properties of undoped, As-doped, and P-doped silicon nanocrystals (Si-Ncs) embedded in a SiO_2 matrix have been investigated using atom probe tomography. It turns out that both As and P atomic distributions have the same behavior in such system, withthe efficient incorporation of impurities in the core of Si-Ncs even in the smallest ones (<2 nm). The impurity level measured in Si-Ncs is strongly size-dependent, and statistically, the smallest Si-Ncs can contain the heaviest doping composition. Moreover, this study reveals an influence of the dopant nature on the kinetic growth of Si-Ncs, leading to the clustering of larger nanocrystals in P-doped samples.

INTRODUCTION

Silicon nanocrystal (Si-Nc)-based devices have attracted much attention due to their multiple and much diversified fields of application like in microelectronics,[1,2] photonics,[3] photovoltaics[4,5] and biomedicine.[6,7] The n- or p-type doping allows to adapt these materials for a specific use by adjusting their optical and electrical properties. Both optical and electrical properties of doped Si-Ncs have been extensively studied.[8−11] In fact, single doping[8,12] or co-doping[13,14] with n- and p-type impurities became a classical process to change the indirect band gap of Si-Ncs to direct band gap and to improve the luminescence efficiency. Recently, a particular interest was focused on the localized surface plasmon resonance (LSPR) exhibited by highly doped Si-Ncs. Then, control of the doping level and the size of Si-Ncs should allow to tune the LSPR for an integration with microelectronics or optoelectronics.[15,16] However, these properties seem to be strongly correlated with the structure of the materials and the elaboration technique and especially with the location of the dopants and the doping level of the Si-Ncs. In the case of a bulk material, a pile-up tendency of n-type dopants is well known at the Si/SiO_2 interface.[17] However, at the nanoscale, the surrounding environment of the Si-Ncs seems to have a real importance on the dopant location. Theoretical studies based on total energy calculations have been performed on free-standing Si-Ncs.[18] They have demonstrated a self-purification effect[19] in small Si-Ncs, revealing that, below 2 nm, the dopant impurities tend to be ejected toward the surface. This dopant segregation at the surface of free-standing Si-Ncs has been evidenced experimentally in the case of P impurities.[20−23] For P-doped Si-Ncs, grown in a microwave plasma reactor, it has been shown that P concentration in Si-Ncs decreased abruptly by reducing the surface native oxide with a wet chemical etching process. This indicates that P atoms segregate at the surface during the growth of Si-Ncs, forming a highly doped thin surface shell.[20,21] Concerning B doping, a same procedure revealed that B atoms are distributed through the entire Si-Nc.[23] However, contrasting results have been evidenced in the case of embedded Si-Ncs, and studies have highlighted that, in small Si-Ncs (1−1.5 nm), p-type dopants (B) are preferentially located at the Si/SiO_2 interface, whereas n-type dopants (P) are energetically favored to be placed in the Si-Nc core.[24,25] Besides, the presence of P or B impurities in the silicon-rich oxide during the growth of Si-Ncs leads to an increase in their

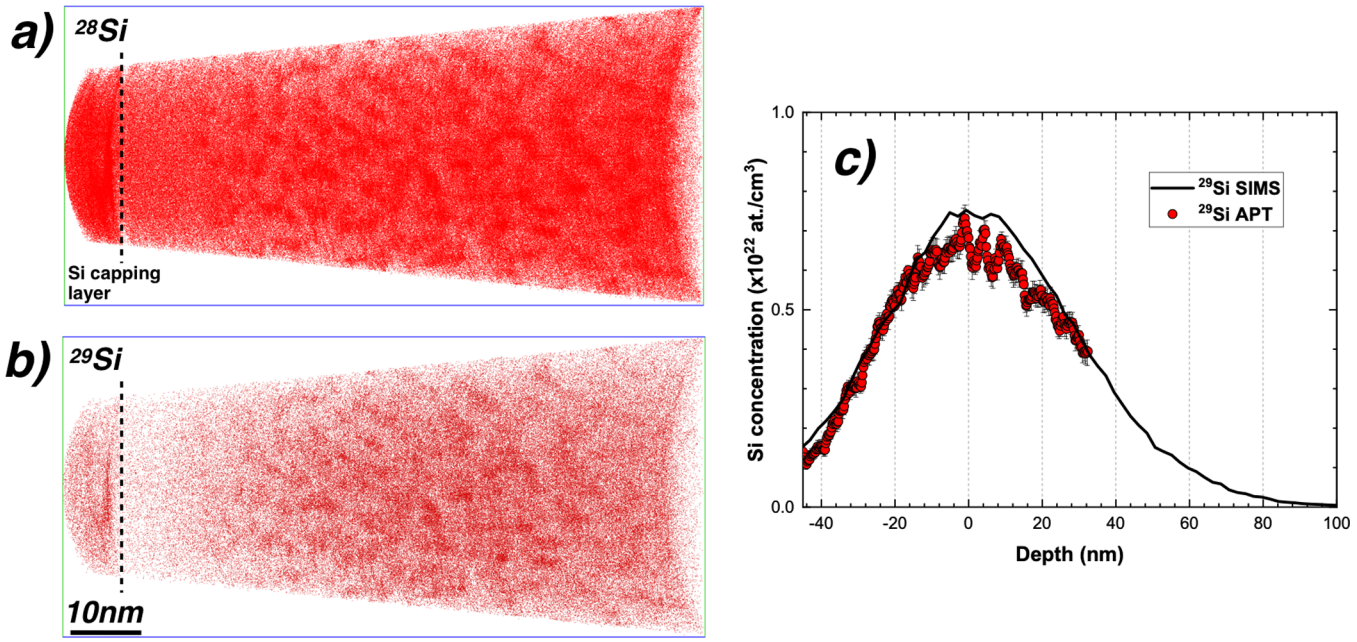

Figure 1. (a, b) 3D distribution of (a) ^{28}Si atoms and (b) ^{29}Si atoms in undoped samples. The analyzed volume is 42 × 42 × 90 nm^3. (c) Depth composition profile measured by SIMS (black solid line) and APT (red circles) representing ^{29}Si composition. The APT profile has been computed in a sampling volume of 20 × 20 × 86 nm^3.

size, revealing an impact of the dopant on the diffusion length of Si atoms.[26] Recently, the trapping of P atoms by Si-Ncs embedded in a SiO_2 matrix has been studied by decoupling the nanocrystal formation and the P diffusion.[27] It has been evidenced that a high level of P impurities (around 6%) can be introduced in the Si-Nc core, without changes on the size distribution. This high doping level of nanocrystals is explained by an increase in the impurity solubility in the nanostructure when decreasing the size. Moreover, the incorporation of P atoms in Si-Ncs (2−5 nm) has been confirmed by atom probe tomography (APT) experiments on P-doped silicon-rich oxynitride (SRON) elaborated by plasma-enhanced chemical vapor deposition (PECVD).[28,29] In these studies, the proxigram analysis has been used to show the location of the dopant in the thin layer. In both cases, it evidenced the presence of P dopants in the core of nanocrystals with a significant P enrichment at the Si/SiO_2 interface.

As P doping in Si-Ncs has been largely studied, we propose here to enlarge the study of n-type doping of nanocrystals by comparing the structural properties of two dopants species, P and As. This investigation has been carried out on undoped and doped Si-Ncs embedded in SiO_2 thin layers elaborated by ion implantation using atom probe tomography. The use of APT allows us to perform the deep structural analysis at the atomic scale of the co-implantation of Si and As or P in SiO_2 thin layers along the implantation profile. The comparison of Si clustering characteristics (composition, size distribution, etc.) between both dopant species evidenced some similarities such as the location of impurities but highlighted a strong dependence of the Si crystal growth on the dopant nature. Moreover, statistical investigation of cluster composition highlighted the possibility to form small nanocrystals with a high level of impurities in both cases.

EXPERIMENTAL SECTION

Undoped, As-doped, and P-doped silicon-rich silicon oxide films were elaborated by using an ion beam synthesis process. Silicon wafers (^{28}Si) were oxidized to form 200 nm-thick $^{28}SiO_2$ films and were implanted with ^{29}Si at 50 keV at a dose of 6 × 10^{16} cm^{-2}. Then, ^{75}As and ^{31}P were implanted at 100 and 50 keV, respectively, in order to match with the projection range of ^{29}Si. For each dopants, the dopant dose was equal to 5 × 10^{15} cm^{-2}. Finally, samples were annealed at 1100 °C for 4 h in pure N_2. A detailed description of the sample preparation is given in ref 11. Based on these implantation parameters and SRIM simulations,[30] a projection range of 70 nm and a total implantation thickness of almost 100 nm are expected for each dopants (^{75}As, ^{31}P, and ^{29}Si).

Time-of-flight secondary ion mass spectrometry (Tof-SIMS) was performed on an Ion TOF SIMS5 (ION-TOF GmbH) using a Cs^+ gun (2 keV, 63 nA, rate of 0.45 nm·s^{-1} in SiO_2) for sputter removal and a Bi^+ liquid metal ion gun (25 keV, 15 nA) for analysis.

The structural and chemical analyses of each samples were performed by atom probe tomography. APT works as a three-dimensional (3D) high-resolution analytical microscope that allows the 3D structural and chemical mapping of a sample at the atomic scale. The process of APT is based on the field evaporation effect produced on surface atoms in a tip-shaped sample with a curvature radius lower than 50 nm. The APT experiment were conducted using a laser-assisted wide-angle tomographic atom probe (LAWATAP, Cameca) with a femtosecond UV pulsed laser (λ = 343 nm) and a detector yield of 0.62. The analyses were performed in a high-vacuum chamber at 10^{-10} mbar at a temperature of 80 K. The preparation of sharp-needled tips was performed using a dual-beam Zeiss NVision 40 FIB-SEM by employing the lift-out and annular milling method.[31] The 3D reconstruction and data analysis were done using home-built GPM3Dsoft software. 3D reconstructions were performed using a method based on an

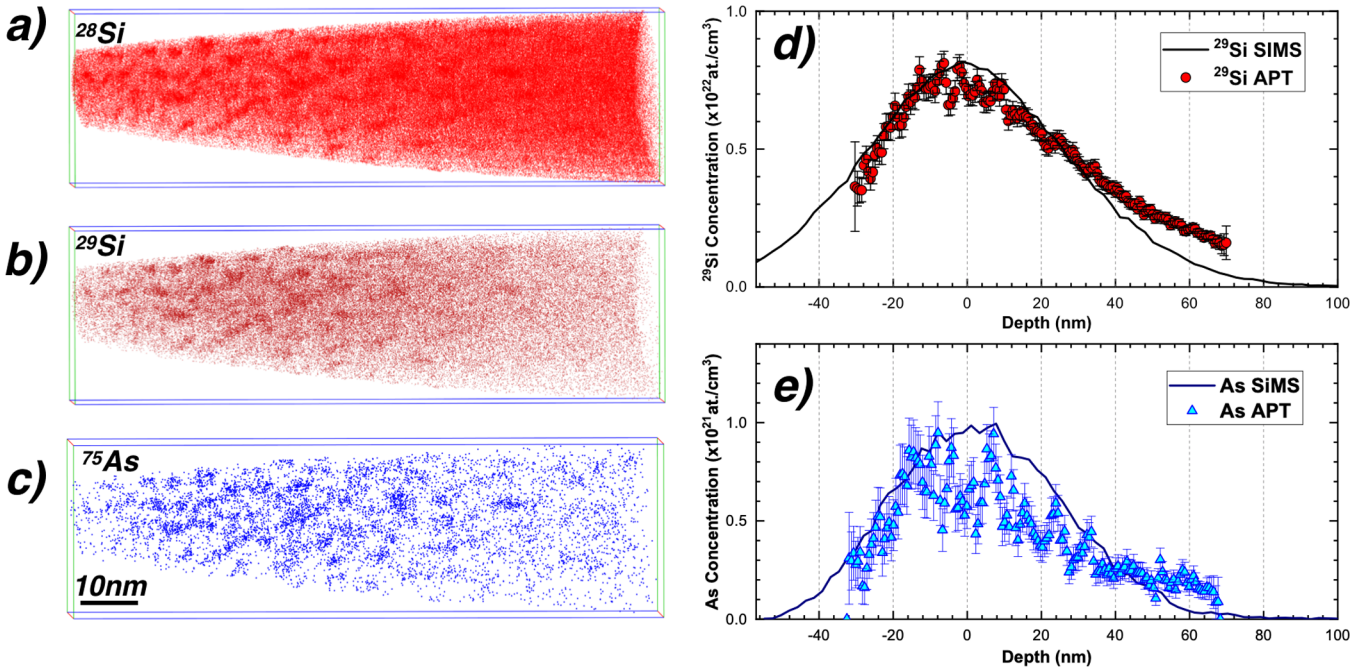

Figure 2. (a–c) 3D distribution of (a) ^{28}Si atoms, (b) ^{29}Si atoms, and (c) As atoms in the As-doped sample. The analyzed volume is 30 × 30 × 101 nm^3. (d, e) Depth composition profile measured by SIMS (solid lines) and APT (symbols) representing (d) ^{29}Si and (e) As composition. The APT profile has been computed in a sampling volume of 12 × 12 × 100 nm^3.

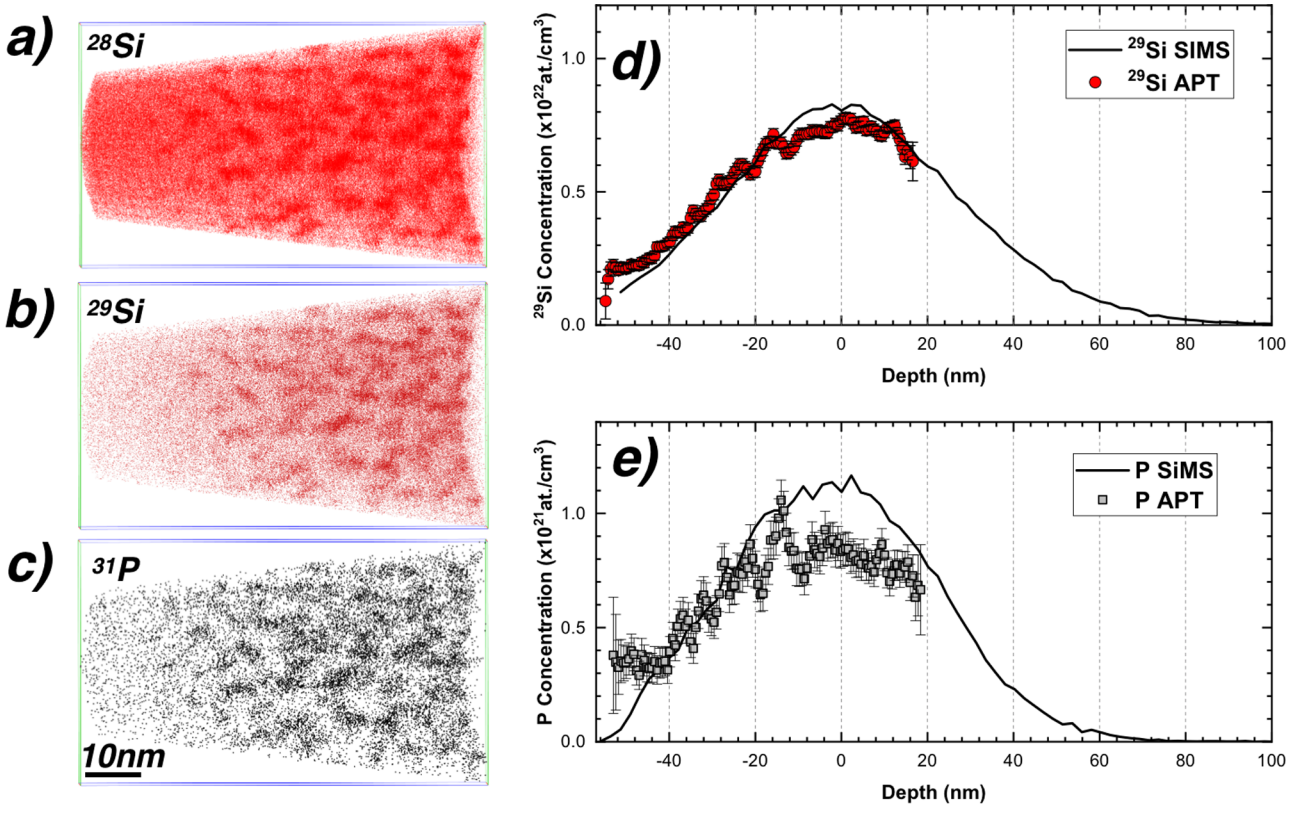

Figure 3. (a–c) 3D distribution of (a) ^{28}Si atoms, (b) ^{28}Si atoms, and (c) P atoms in the P-doped sample. The analyzed volume is 43 × 43 × 72 nm^3. (d, e) Depth composition profile measured by SIMS (solid lines) and APT (symbols) representing (d) ^{29}Si and (e) As composition. The APT profile has been computed in a sampling volume of 20 × 20 × 70 nm^3. Note that the profile is not complete as the specimen unfortunately broke during the APT analysis. The APT data set was still sufficient for data extraction and comparison with the As doping.

SEM image of the tip before analysis to determine its curvature radius,[32] then reconstruction parameters were adjusted in order to fit to SIMS concentration profiles of the dopants. It is emphasized that APT is a chemical analysis. Therefore, it does not give any piece of information concerning the possible electrical activation of the dopant. Thus, in the following, when

we use the words "doping" or "dopant", they must be understood as a shortcut for "chemical doping".

RESULTS AND DISCUSSION

The 3D chemical maps obtained on undoped samples are represented in Figure 1a,b for ^{28}Si and ^{29}Si, respectively. For clarity reasons, O atoms are not shown. The spatial distribution of ^{28}Si and ^{29}Si atoms highlights that, after the annealing treatment performed at 1100 °C, the implantation of ^{29}Si leads to the formation of silicon clusters consisting of ^{28}Si and ^{29}Si atoms without distinction. To ensure the accuracy of APT reconstruction, depth composition profiles of ^{29}Si atoms have been computed, based on the APT analysis, and compared to SIMS measurements. In fact, recent studies on different materials have revealed that APT can provide accurate implanted species mapping by comparing APT results with more conventional analysis techniques like SIMS.[33−35] Figure 1c displays an overlaid image of SIMS and APT depth composition profiles for ^{29}Si. The zero position has been set to correspond to the peak center of the implantation profile. SIMS measurement evidences that the region of interest, corresponding to the implantation range of ^{29}Si in the $^{28}SiO_2$ thin films, of almost 110 nm of thickness, centered at 55 nm from the thin film surface. The APT profile of ^{29}Si shows a maximum composition of 6.8×10^{21} atoms/cm^3 (10.3 atom %) at the peak of the implantation profile.

Concerning doped samples, the 3D chemical maps obtained on As-doped thin layers are represented in Figure 2a−c for ^{28}Si, ^{29}Si, and As atoms, respectively. Regarding the spatial distribution of ^{28}Si and ^{29}Si atoms observed in Figure 2a,b, the annealing treatment performed at 1100 °C leads to the formation of silicon clusters as it was observed in undoped samples. At the same time, regarding the spatial distribution of As atoms in the analyzed volume (Figure 2c), As atoms tend to aggregate at these same Si-Nc locations. Figure 2d,e displays overlaid images of SIMS and APT depth composition profiles for ^{29}Si and As, respectively.

SIMS measurements confirms an implantation of both impurities, As and ^{29}Si, in the same region of the thin films. The doses of implanted As atoms have been measured in APT and SIMS analyses by integrating over the length of the analyzed volume in both cases. The measured doses are $\phi^{As}_{APT} = 4.3 \times 10^{15}$ cm^{-2} and $\phi^{As}_{SIMS} = 5.1 \times 10^{15}$ cm^{-2}. The difference observed between both analysis methods can be explained by the size of the volume used during the analyses, which is far below in the APT experiment. In these conditions, the highest compositions reached by ^{29}Si and As in the $^{28}SiO_2$ thin layer are 7.5×10^{21} atoms/cm^3 (11 atom %) and 8×10^{20} atoms/cm^3 (1.3 atom %), respectively. Then, toward the extremities of the depth profile, both compositions decrease slowly.

For the P-doped sample, the spatial distribution of ^{28}Si, ^{29}Si, and P atoms and the depth profile of dopant composition are represented in Figure 3. As previously observed for the As-doped sample, the formation of clusters composed of ^{28}Si, ^{29}Si, and P can also be observed (Figure 3a−c). SIMS measurements in Figure 3d,e evidence a same implantation range for ^{29}Si and P, respectively, and a similar region of interest as observed in undoped and As-doped samples. In this layer, the maximum compositions of ^{29}Si and P reach their maximum at 7.5×10^{21} atoms/cm^3 (11 atom %) and 8×10^{20} atoms/cm^3 (1.2 atom %), respectively. The doses measured for the P-doped sample are $\phi^{P}_{APT} = 2.7 \times 10^{15}$ cm^{-2} and $\phi^{P}_{SIMS} = 3.7 \times 10^{15}$ cm^{-2}. It is worth noting that for the P-doped sample, only a part of the region of interest has been evaporated during the APT experiment. Therefore, considering the size and the quasi-symmetry of the SIMS peak shape, the size of the analyzed volume with APT must be enough to compare the doping in both samples. Globally, the structural evolution of the As-doped and P-doped samples seems to be equivalent, with an aggregation of the impurities at the same position than the clustering of Si atoms and a similar evolution of the implanted species after the annealing process.

Theoretically, the implantation of ^{29}Si at 50 keV at a dose of 6×10^{16} cm^{-2} and implantation of P at 50 keV and As at 100 keV at a dose of 5×10^{15} cm^{-2} should lead to a maximum composition of 15 atom % for ^{29}Si and 1.5 atom % for P and As in the center of the implantation profile and before the annealing treatment. The concentration profiles presented in Figures 2d and 3d show a smaller value. This lower measured composition is explained by the diffusion of the implanted species during the annealing treatment.

The APT experiment not only gives an overview of the thin layer nanostructure but also allows to perform deeper investigation on the structural properties, especially on the precise dopant location and the Si-Nc characteristics. To do so, clusters observed in the 3D reconstruction (Figures 1−3) have been identified by using a cluster detection algorithm. Then, to compute the size and the composition of each nanoparticles, the Si-Ncs were considered as spherical nanoparticles as it is commonly observed in the TEM analysis in these kind of samples.[36] The number of Si and the number of As or P atoms of previously defined clusters are counted and corrected from the detector yield. Another correction is carried out in order to correct the effect of the local magnification[37] that tend to artificially include Si, O as well as As or P atoms from the matrix into the Si-Ncs during the reconstruction step, following the procedure established for similar samples.[38] This effect is well known in the case of the Si/SiO_2 interface due to a large difference in the evaporation field required between these phases and had already been evidenced in several studies.[28,29,38] We have assumed that a fraction of As or P atoms of the matrix is artificially introduced into the Si-Ncs. This fraction has been determined from the behavior of oxygen atoms and a previous work.[38] Finally, the diameter of each Si-Ncs was computed by considering the number and the size of Si and dopants (As or P).

Figure 4a−c displays the size distribution of Si-Nc diameter measured in undoped, As-doped, and P-doped thin layers, respectively. A difference in diameter distribution shape can be noticed between undoped and As-doped samples on one side and P-doped samples on the other side. Considering the case of the undoped and As doping, the size distribution of Si-Ncs has been fitted with a lognormal distribution (Figure 4a), whereas in the case of P doping, a Gaussian distribution has been required to fit the size distribution (Figure 4b). The non-uniform concentration profiles carried out by the implantation process and the long annealing treatment should favor the lognormal size-distribution shape.[39] Nevertheless, a Gaussian distribution shape has already been reported in the case of undoped Si-Ncs elaborated by ion implantation in almost the same conditions.[40] The mean diameter of Si-Ncs in the undoped sample is 2.5 ± 0.6 nm, while it was measured at 2.5 ± 0.4 nm for As doping. These diameters are consistent with those measured in undoped Si-Ncs grown by ion beam synthesis in an equivalent range of elaboration conditions.[41−44]

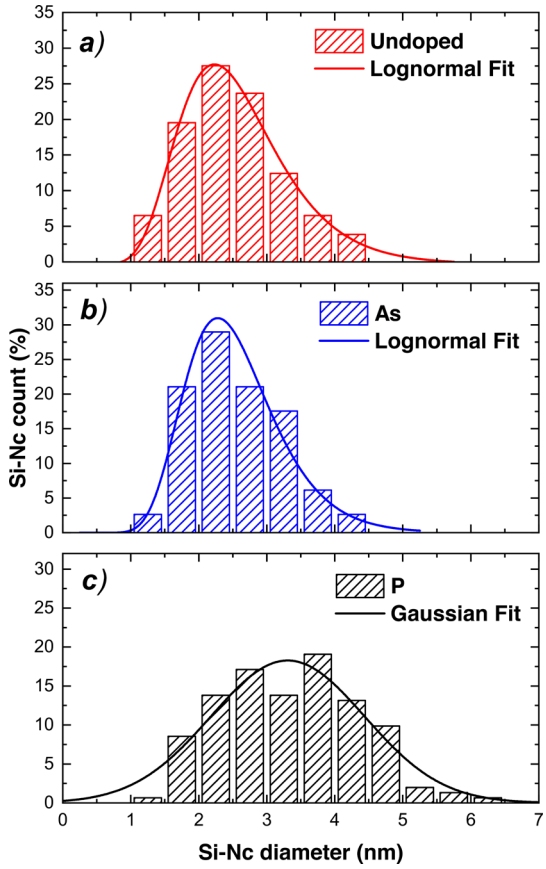

Figure 4. Size distribution of Si-Nc diameter of the (a) undoped sample, (b) As-doped sample, and (c) P-doped sample. Solid lines represent the curve fitting of the size distribution.

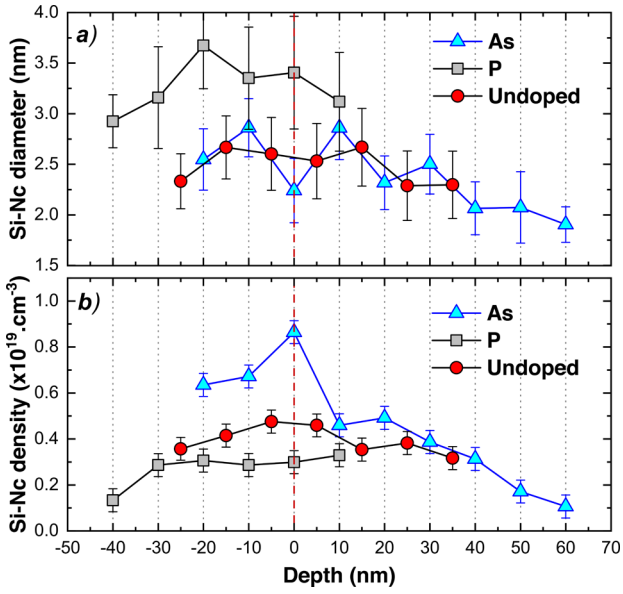

Figure 5. (a) Mean Si-Nc diameter of P-doped (gray squares), As-doped (cyan triangles), and undoped (red circles) samples and (b) density of Si-Ncs of P-doped, As-doped, and undoped samples computed in 10 nm deep boxes along the analyzed volume. The zero position represents the peak of the implantation profile.

For instance, it has been reported, by XRD analysis, that similar implantation conditions of Si in SiO_2 (dose of 5×10^{16} cm^{-2} at 50 keV, annealing at 1100 °C) lead to the formation of Si-Ncs with a diameter of 2.4 nm.[41] In the case of P doping sample, the size distribution is wider, and the mean diameter of Si-Ncs is larger and was measured to be about 3.3 ± 1.0 nm. These differences between the two chemical elements may indicate that the nature of the dopant has a direct influence on the diffusion parameter and Si-Nc growth process during the annealing treatment. Here, it shows that introduction of P atoms tend to change these parameters while introduction of As atoms does not have any impact on Si-Nc growth. In fact, in P-doped systems, the increase in the Si-Nc size compared to undoped samples is often attributed to longer diffusion length of Si atoms in the presence of P atoms, which allows the growth of larger Si-Ncs.[26,45]

The analyzed volumes have been splitted in a sampling volume of 10 nm in depth in the direction of the APT analysis. This allowed us to investigate the evolution of the size distribution and the density of Si-Ncs along the implantation profile (Figure 5). In this figure, Si-Nc characteristics for undoped, As-doped, and P-doped samples have been superimposed on the basis of SIMS measurements represented in Figures 1−3. The zero position has been set to correspond to the peak position of the dopant profile. Figure 5a represents the evolution of the mean diameter along the depth profile in undoped, As-doped, and P-doped samples. It clearly highlights a similar evolution of Si-Nc diameter along the implantation profile between undoped and As-doped thin layers. Moreover, in each case, we can notice that the mean diameter of Si-Ncs tends to decrease by a few tens of nanometers at the edges of the implantation profile and reach their maximum near to the center of the implantation profile. The decrease in the Si-Nc size at the edges of the implantation shape is an expected effect. In fact, larger Si-Ncs are expected to grow at the implantation peak, where the silicon excess concentration reaches its maximum. However, in our case, the difference in Si-Nc diameter is limited, and only a slight decrease is observed by moving away from the implantation peak. APT reconstructions showed that large and small Si-Ncs are observable along the implantation profile. The densities of Si-Ncs displayed in Figure 5b, for the undoped, P-doped, and As-doped samples, show that, near the middle range of the implantation profile, the density of nanocrystals in undoped and As-doped thin layers reaches values from 4×10^{18} to 8×10^{18} nanocrystals/cm^3, which are higher compared to the value measured in the P-doped sample (3×10^{18} nanocrystals/cm^3). However, at the edges of the implantation profile, Si-Nc densities are similar. These results are in accordance with the evolution of the ^{29}Si excess presented in Figure 2d and 3d. As the mean diameter does not strongly change along the analysis direction, the presence of a higher silicon excess in the middle of the implantation must allow the formation of more numerous Si-Ncs. Moreover, knowing that all samples have been elaborated in the same condition, the clustering of smaller nanocrystals, in average, in undoped and As-doped samples, should lead to the formation of a larger number of Si-Ncs than in the case of the P doping. The difference observed between undoped and As-doped Si-Nc densities, at the left side of the implantation peak, may be explained by the tip shape, inducing a smaller analyzed volume for the As-doped sample.

Concerning the doping efficiency of Si-Ncs in As-doped and P-doped thin layers, Figure 6a,b provides two cross sections of As and P implantation in SiO_2, respectively. This displays a first insight into the impurities in the matrix, revealing that the majority of As atoms (blue dots) and P atoms (black dots) are

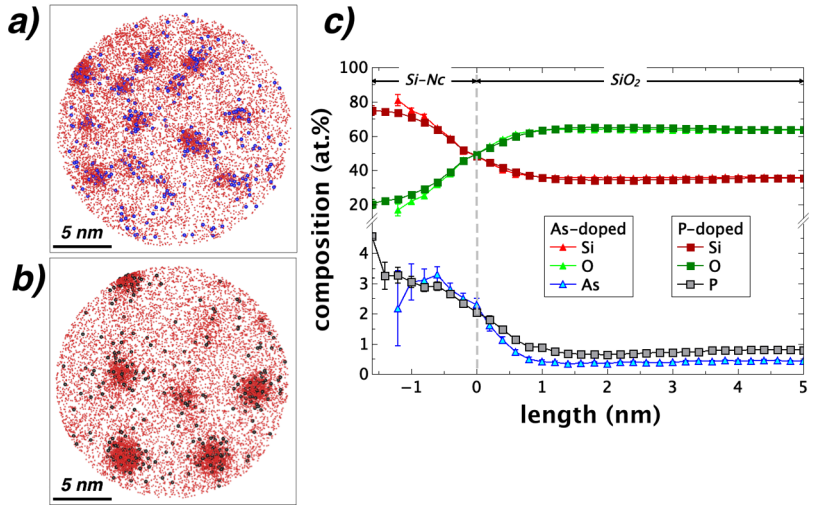

Figure 6. (a, b) Cross sections of (a) As-doped and (b) P-doped samples. In (a), blue and red dots correspond to As and Si atoms, respectively (volume is 22 × 22 × 3 nm^3). In (b), black and red dots correspond to P and Si atoms, respectively (volume is 22 × 22 × 3 nm^3). (c) Erosion profile of As-doped and P-doped samples.

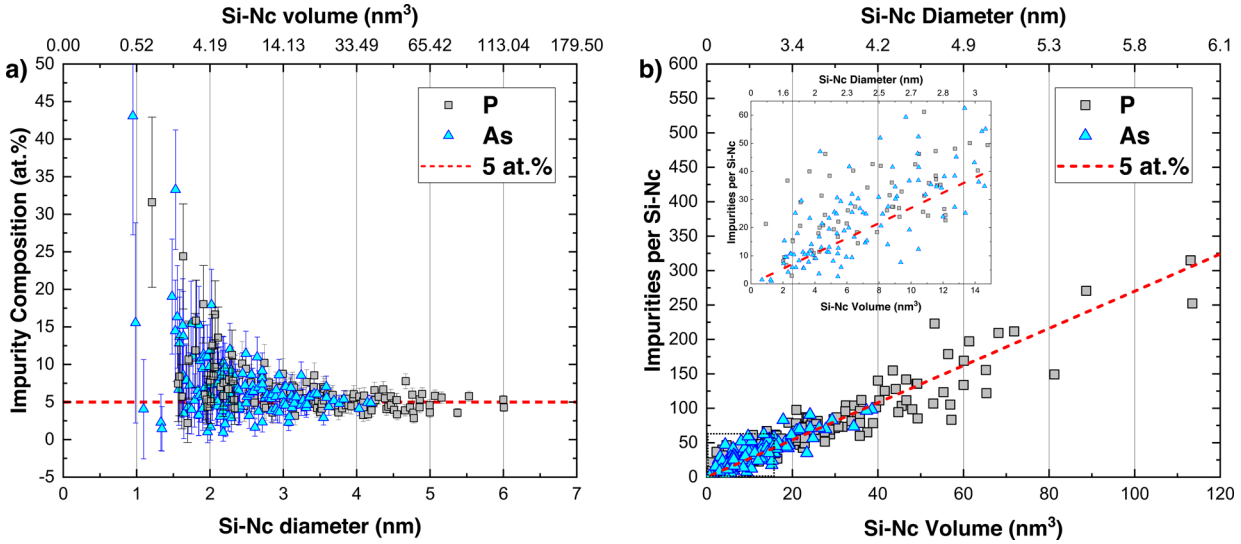

Figure 7. (a) Impurity composition of each Si-Ncs as a function of their diameter. (b) Number of impurity per Si-Ncs as a function of their volume. Inset shows a zoom-in image for the smallest Si-Ncs.

well concentrated in the Si-Nc regions. The atomic fraction of impurities in the Si-Ncs has been estimated, showing that 68% and 55% of As and P atoms, respectively, are located in the Si-Ncs. The rest of impurities are diluted in the SiO_2 matrix and correspond to a concentration of 1.5×10^{20} atoms/cm^{-3} for As and 2.5×10^{20} atoms/cm^{-3} for P. The exact location of dopants around the Si-Ncs in both samples has been investigated by computing the erosion profile,[46,47] as represented in Figure 6c. Erosion profiles show the evolution of the composition measured from the center to the surrounding matrix of clusters. These profiles have been computed by considering all the clusters present in the analyzed volumes (Figures 2a and 3a). The O profile reveals the measurement of almost 20 atom % of O in the core of Si-Ncs. This low O level is the result of the local magnification effect[37] between Si and SiO_2 phases as described previously. In these samples, Si-Ncs are pure. As and P erosion profiles highlight that both n-type dopants are incorporated in the core of Si-Ncs. The raw data show (Figure 6c), in both samples, an impurity composition reaching 3 atom % in the core of Si-Ncs. This measurement is strongly affected by the local magnification effect, that is, artificial introduction of atoms originating from the surrounding matrix in the clusters, which artificially decrease the measured concentration of As or P in the core of the clusters. By applying the correction model proposed by Talbot et al.,[38] we have corrected the concentration of each Si-Ncs. The real mean impurity concentration in all Si-Ncs can be estimated at 5 to 6 atom %. Similar profiles (not shown here) were computed as a function of the diameter of Si-Ncs (with a class diameter of 1 nm). It did not evidence any influence of the Si-Nc diameter on the impurity introduction and location. The absence of the pile-up effect of dopants at Si/SiO_2 is evidenced, allowing us to conclude that the self-purification effect does not occur in this system. Consequently, a strong number of impurity atoms can be expected to be incorporated in the Si-Ncs in the range of diameter (1−5 nm) of our samples.

Finally, the impurity composition of each Si-Ncs have been computed for both samples. The impurity composition (As and P) in each Si-Ncs as a function of the Si-Nc diameter (or volume) is presented in Figure 7a. All Si-Ncs detected in the APT analysis contain P or As atoms (152 and 147 Si-Ncs were detected in P-doped and As-doped samples, respectively). It is worth noting that both kinds of dopant tend to have the same behavior in terms of impurity level in the Si-Ncs (red dashed line in Figure 7a). In fact, regardless of the dopant nature, the doping of the larger Si-Ncs (above 3 nm) seems to reach an equilibrium state with an impurity level of 5 to 6 atom %. These values are far above than the expected values considering the solid solubility of P and As in bulk Si (0.5 to 1 atom %).[48] For the smallest Si-Ncs (below 2 nm), we observe the large dispersion of impurity level in the core of Si-Ncs. However, the majority of these nanocrystals exhibit a higher doping level than the equilibrium one of 5 atom %, which reaches values from 10 to 45 atom % (see inset of Figure 7b). Moreover, this result clearly evidences a size dependency of the impurity level in the core of the Si-Ncs. In order to quantify the number of impurities introduced in the core of these Si-Ncs, the number of dopants (As or P) belonging to each Si-Ncs is represented in Figure 7b as a function of the volume of these Si-Ncs. The red dashed line in Figure 7b represents the number of impurity required to reach a mean impurity composition of 5 atom % (i.e., 2.5×10^{21} atoms/cm^3) in the Si-Ncs, corresponding to the equilibrium state established in Figure 7a and reached for larger Si-Ncs. For both kinds of impurities, this proportional relationship between the impurity number incorporated in Si-Ncs and their volume seems to fit the entire data points. However, for the smaller Si-Ncs (below 3 nm), the inset of Figure 7b shows that, for the majority of Si-Ncs, the number of impurity introduced is higher than this "equilibrium state" line. This clearly confirms a size dependency of the doping level in Si-Ncs, showing that formation of highly doped small Si-Ncs may be performed.

DISCUSSION

The doping of Si-Ncs embedded in SiO_2 with n-type dopants has been extensively studied, relying on the example of P doping.[26,28,29,49] Here, the comparison between two n-type dopants (P and As) in Si-Ncs elaborated by ion beam synthesis allowed us to evidence that similarities exist in these n-type dopants, especially on the location and the concentration of impurities introduced in the core of Si-Ncs. However, it reveals that some major changes can be expected on the growth kinetics of the Si-Ncs, depending on the nature of the dopant.

The elaboration of Si-Ncs embedded in SiO_2 by co-implantation of ^{29}Si and As or P atoms have been performed in equal conditions. These parameters allowed the implantation of dopants in the same projection range, with a comparable composition. Nevertheless, the APT analyses highlight two significantly different size distributions of Si-Ncs. Larger Si-Nc diameters have been measured in the P-doped sample compared to the As-doped sample. Some studies carried out on the doping of Si-Ncs have shown that, compared to the undoped SiO_x layer, the doping with species like P or B leads to the growth of larger Si-Ncs.[26,45] This is explained by the softening of the matrix produced by the presence of dopants during the clustering of Si. This leads to an increase in the diffusion length of Si, which allows the formation of larger Si-Ncs and induces a broader size distribution of Si-Ncs. Here, we evidenced a clear difference in the average diameter of Si-Ncs between As and P doping. This can be interpreted by considering that the diffusion length of Si atoms in the presence of P atoms should be higher than that in the presence of As atoms. This effect may induce the difference in distribution shape observed between both samples. In fact, in the case of ionic implantation synthesis, the non-uniformity of the profile of the implanted species and their possible diffusion in a "free region" (outside of the implantation), after annealing, lead to a lognormal shape of the size distribution of the nanoparticles.[39] This kind of distribution shape has been reported for the growth of Si-Ncs in silica after Si implantation.[50−52] In the case of a As doping, the measured diameter of Si-Ncs with APT is equivalent to the Si-Nc diameter measured in the undoped thin layer elaborated with the same conditions. Moreover, both are in accordance with studies carried out with other analysis techniques on similar materials.[41−43] Then, compared to the case of P,[26,45] As do not significantly change the diffusion length of Si, and the resulting size distribution presents a lognormal shape as it has been shown in the case of undoped samples. In contrary, in P-doped samples, due to the longer diffusion length of Si in the host matrix, the nucleation of Si should appear faster with lesser strains and a weaker importance of the implantation profile on the growth of Si-Ncs, leading to a Gaussian shape of the size distribution.

Therefore, from a pure doping level point of view, both n-type dopants evolve in the same way. In fact, the APT analyses of As-doped and P-doped Si-Ncs revealedthe efficient incorporation of impurities in the core of the Si-Ncs (Figure 6), even in the smallest ones. In the case of free-standing Si-Ncs, it has been shown that, due to the self-purification effect,[18,19] the dopants should be expelled toward the surface when the size of Si-Ncs decrease. Therefore, in the case of embedded Si-Ncs, behavior can be different depending on the surrounding matrix. For instance, it is worth noting that some other APT investigations performed on the P doping of SRON matrices elaborated by PECVD clearly show different results.[28,29] In these systems, a significant enrichment of the dopant composition appears at the Si-Ncs/SiO_2 interface, demonstrating the existence of the self-purification effect. Consequently, only a low level of impurity is incorporated in the core of the Si-Ncs. However, their investigations, made on P-doped SiO_x layers elaborated by PECVD,[52] evidenced an effective incorporation of P in the core of Si-Ncs without any enrichment at the interface. This confirms the importance of the surrounding matrix on the dopant location in the Si-Ncs. In Si-Ncs surrounded by a SiO_2 shell, the location of P atoms in the core of Si-Ncs is favored because of the large diffusion barrier formed by SiO_2[24] and of the lower energy required to form the P−Si bond than the P−O bond.[53] Concerning the concentration of dopants in Si-Ncs, due to the higher solubility of As in bulk Si,[48] one can expect to find a higher doping level in Si-Ncs. However, a similar evolution of the composition has been evidenced as a function of the Si-Nc diameter, showing that larger Si-Ncs, above 3 nm, tend to reach an equilibrium composition of doping of about 5 to 6 atom %. Here, the absence of self-purification shows that a large amount of dopants can be incorporated in Si-Ncs of all sizes without distinction. In fact, if larger Si-Ncs reach an average composition value, then the smallest ones, below 2 nm, can statistically get a much higher doping level (from 10 to 45 atom %). It is worth noting that these compositions

correspond to a large number of impurities that are incorporated in the Si-Ncs in both n-type dopants.

CONCLUSIONS

The structural characteristics of As-doped and P-doped Si-Ncs embedded in SiO_2 elaborated by ion implantation have been investigated. The comparison between two n-type dopants reveals similarities in terms of dopant location. It allows to evidence the incorporation of dopants in the core of Si-Ncs. For both kinds of dopants, in contrast with the self-purification effect, when the size of the Si-Ncs decreases, the doping level tends to increase, leading to the possibility to form heavily doped small Si-Ncs. However, a different impact of the nature of the dopant on the kinetic growth of Si-Ncs has been highlighted. The presence of P atoms during the formation of clusters tends to increase the diffusion length of Si atoms, while that of As atoms seems to decrease it. The outcome is the growth of smaller but more numerous Si-Ncs in the case of As doping and leads to significant differences in the shape of the size distribution of Si-Ncs between the two samples.

AUTHOR INFORMATION

Corresponding Author

*E-mail: etienne.talbot@univ-rouen.fr. Phone: +33 (0)2 32 95 51 32.

REFERENCES

(1) Tiwari, S.; Rana, F.; Hanafi, H.; Hartstein, A.; Crabbé, E. F.; Chan, K. A Silicon Nanocrystals Based Memory. *Appl. Phys. Lett.* **1996**, *68*, 1377−1379.

(2) Talapin, D. V.; Lee, J.-S.; Kovalenko, M. V.; Shevchenko, E. V. Prospects of Colloidal Nanocrystals for Electronic and Optoelectronic Applications. *Chem. Rev.* **2010**, *110*, 389−458.

(3) Khriachtchev, L.; Ossicini, S.; Iacona, F.; Gourbilleau, F. Silicon Nanoscale Materials: From Theoretical Simulations to Photonic Applications. *Int. J. Photoenergy* **2012**, 872576.

(4) Green, M. A. Third Generation Photovoltaics: Ultra-High Conversion Efficiency at Low Cost. *Progr. Photovolt.: Res. Appl.* **2001**, *9*, 123−135.

(5) Conibeer, G.; Green, M.; König, D.; Perez-Wurfl, I.; Huang, S.; Hao, X.; Di, D.; Shi, L.; Shrestha, S.; Puthen-Veetil, B.; et al. Silicon Quantum Dot Based Solar Cells: Addressing the Issues of Doping, Voltage and Current Transport. *Progr. Photovolt.: Res. Appl.* **2011**, *19*, 813−824.

(6) O'Farrell, N.; Houlton, A.; Horrocks, B. R. Silicon Nanoparticles: Applications in Cell Biology and Medicine. *Int. J. Nanomed.* **2006**, *1*, 451.

(7) Cheng, X.; Lowe, S. B.; Reece, P. J.; Gooding, J. J. Colloidal Silicon Quantum Dots: from Preparation to the Modification of Self-Assembled Monolayers (SAMs) for BioApplications. *Chem. Soc. Rev.* **2014**, *43*, 2680−2700.

(8) Fujii, M.; Mimura, A.; Hayashi, S.; Yamamoto, Y.; Murakami, K. Hyperfine Structure of the Electron Spin Resonance of Phosphorus-Doped Si Nanocrystals. *Phys. Rev. Lett.* **2002**, *89*, 206805.

(9) Fujii, M.; Mimura, A.; Hayashi, S.; Yamamoto, K. Photoluminescence from Si Nanocrystals Dispersed in Phosphosilicate Glass Thin Films: Improvement of Photoluminescence Efficiency. *Appl. Phys. Lett.* **1999**, *75*, 184−186.

(10) Sumida, K.; Ninomiya, K.; Fujii, M.; Fujio, K.; Hayashi, S.; Kodama, M.; Ohta, H. Electron Spin-Resonance Studies of Conduction Electrons in Phosphorus-Doped Silicon Nanocrystals. *J. Appl. Phys.* **2007**, *101*, No. 033504.

(11) Khelifi, R.; Mathiot, D.; Gupta, R.; Muller, D.; Roussel, M.; Duguay, S. Efficient N-Type Doping of Si Nanocrystals Embedded in SiO_2 by Ion Beam Synthesis. *Appl. Phys. Lett.* **2013**, *102*, No. 013116.

(12) Sato, K.; Niino, K.; Fukata, N.; Hirakuri, K.; Yamauchi, Y. The Synthesis and Structural Characterization of Boron-Doped Silicon-Nanocrystals with Enhanced Electroconductivity. *Nanotechnology* **2009**, *20*, 365207.

(13) Fujii, M.; Yamaguchi, Y.; Takase, Y.; Ninomiya, K.; Hayashi, S. Control of Photoluminescence Properties of Si Nanocrystals by Simultaneously Doping n- and p-Type Impurities. *Appl. Phys. Lett.* **2004**, *85*, 1158−1160.

(14) Fujii, M.; Yamaguchi, Y.; Takase, Y.; Ninomiya, K.; Hayashi, S. Photoluminescence from Impurity Codoped and Compensated Si Nanocrystals. *Appl. Phys. Lett.* **2005**, *87*, 211919.

(15) Pi, X.; Delerue, C. Tight-Binding Calculations of the Optical Response of Optimally P-Doped Si Nanocrystals: A Model for Localized Surface Plasmon Resonance. *Phys. Rev. Lett.* **2013**, *111*, 177402.

(16) Zhou, S.; Pi, X.; Ni, Z.; Ding, Y.; Jiang, Y.; Jin, C.; Delerue, C.; Yang, D.; Nozaki, T. Comparative Study on the Localized Surface Plasmon Resonance of Boron- and Phosphorus-Doped Silicon Nanocrystals. *ACS Nano* **2015**, *9*, 378−386.

(17) Sakamoto, K.; Nishi, K.; Ichikawa, F.; Ushio, S. Segregation and Transport Coefficients of Impurities at the Si/SiO_2 Interface. *J. Appl. Phys.* **1987**, *61*, 1553−1555.

(18) Chan, T.-L.; Tiago, M. L.; Kaxiras, E.; Chelikowsky, J. R. Size Limits on Doping Phosphorus into Silicon Nanocrystals. *Nano Lett.* **2008**, *8*, 596−600.

(19) Dalpian, G. M.; Chelikowsky, J. R. Self-Purification in Semiconductor Nanocrystals. *Phys. Rev. Lett.* **2006**, *96*, 226802.

(20) Stegner, A. R.; Pereira, R. N.; Lechner, R.; Klein, K.; Wiggers, H.; Stutzmann, M.; Brandt, M. S. Doping Efficiency in Freestanding Silicon Nanocrystals from the Gas Phase: Phosphorus Incorporation and Defect-Induced Compensation. *Phys. Rev. B* **2009**, *80*, 165326.

(21) Rowe, D. J.; Jeong, J. S.; Mkhoyan, K. A.; Kortshagen, U. R. Phosphorus-Doped Silicon Nanocrystals Exhibiting Mid-Infrared Localized Surface Plasmon Resonance. *Nano Lett.* **2013**, *13*, 1317−1322.

(22) Pi, X. D.; Gresback, R.; Liptak, R. W.; Campbell, S. A.; Kortshagen, U. Doping Efficiency, Dopant Location, and Oxidation of Si Nanocrystals. *Appl. Phys. Lett.* **2008**, *92*, 123102.

(23) Lechner, R.; Stegner, A. R.; Pereira, R. N.; Dietmueller, R.; Brandt, M. S.; Ebbers, A.; Trocha, M.; Wiggers, H.; Stutzmann, M. Electronic Properties of Doped Silicon Nanocrystal Films. *J. Appl. Phys.* **2008**, *104*, No. 053701.

(24) Guerra, R.; Ossicini, S. Preferential Positioning of Dopants and Co-Dopants in Embedded and Freestanding Si Nanocrystals. *J. Am. Chem. Soc.* **2014**, *136*, 4404−4409.

(25) Garcia-Castello, N.; Illera, S.; Prades, J. D.; Ossicini, S.; Cirera, A.; Guerra, R. Energetics and Carrier Transport in Doped Si/SiO_2 Quantum Dots. *Nanoscale* **2015**, *7*, 12564−12571.

(26) Fujii, M.; Toshikiyo, K.; Takase, Y.; Yamaguchi, Y.; Hayashi, S. Below Bulk-Band-Gap Photoluminescence at Room Temperature from Heavily P- and B-Doped Si Nanocrystals. *J. Appl. Phys.* **2003**, *94*, 1990−1995.

(27) Perego, M.; Seguini, G.; Arduca, E.; Frascaroli, J.; De Salvador, D.; Mastromatteo, M.; Carnera, A.; Nicotra, G.; Scuderi, M.; Spinella,

C.; et al. Thermodynamic Stability of High Phosphorus Concentration in Silicon Nanostructures. *Nanoscale* **2015**, *7*, 14469−14475.
(28) Nomoto, K.; Hiller, D.; Gutsch, S.; Ceguerra, A. V.; Breen, A.; Zacharias, M.; Conibeer, G.; Perez-Wurfl, I.; Ringer, S. P. Atom Probe Tomography of Size-Controlled Phosphorus Doped Silicon Nanocrystals. *Phys. Status Solidi RRL* **2017**, *11*, 1600376.
(29) Gnaser, H.; Gutsch, S.; Wahl, M.; Schiller, R.; Kopnarski, M.; Hiller, D.; Zacharias, M. Phosphorus Doping of Si Nanocrystals Embedded in Silicon Oxynitride Determined by Atom Probe Tomography. *J. Appl. Phys.* **2014**, *115*, No. 034304.
(30) Ziegler, J. F.; Ziegler, M. D.; Biersack, J. P. SRIM − The Stopping and Range of Ions in Matter (2010). *Nucl. Instrum. Methods Phys. Res., Sect. B* **2010**, *268*, 1818−1823.
(31) Thompson, G. B.; Miller, M. K.; Fraser, H. L. Some Aspects of Atom Probe Specimen Preparation and Analysis of Thin Film Materials. *Ultramicroscopy* **2004**, *100*, 25−34.
(32) Lefebvre-Ulrikson, W., Vurpillot, F., Sauvage, X., Eds; *Atom Probe Tomography*: Academic Press, 2016.
(33) Thompson, K.; Bunton, J. H.; Moore, J. S.; Jones, K. S. Compositional Analysis of Si Nanostructures: SIMS−3D Tomographic Atom Probe Comparison. *Semicond. Sci. Technol.* **2007**, *22*, S127.
(34) Duguay, S.; Colin, A.; Mathiot, D.; Morin, P.; Blavette, D. Atomic-Scale Redistribution of Dopants in Polycrystalline Silicon Layers. *J. Appl. Phys.* **2010**, *108*, No. 034911.
(35) Shimizu, Y.; Takamizawa, H.; Kawamura, Y.; Uematsu, M.; Toyama, T.; Inoue, K.; Haller, E.; Itoh, K.; Nagai, Y. Atomic-scale Characterization of Germanium Isotopic Multilayers by Atom Probe Tomography. *J. Appl. Phys.* **2013**, *113*, No. 026101.
(36) Garrido, B.; López, M.; Pérez-Rodriguez, A.; García, C.; Pellegrino, P.; Ferré, R.; Moreno, J. A.; Morante, J. R.; Bonafos, C.; Carrada, M.; et al. Optical and Electrical Properties of Si-Nanocrystals Ion Beam Synthesized in SiO_2. *Nucl. Instrum. Methods Phys. Res., Sect. B* **2004**, *216*, 213−221.
(37) Vurpillot, F.; Bostel, A.; Blavette, D. Trajectory Overlaps and Local Magnification in Three-Dimensional Atom Probe. *Appl. Phys. Lett.* **2000**, *76*, 3127−3129.
(38) Talbot, E.; Lardé, R.; Gourbilleau, F.; Dufour, C.; Pareige, P. Si Nanoparticles in SiO_2 An Atomic Scale Observation for Optimization of Optical Devices. *EPL Europhysics Lett.* **2009**, *87*, 26004.
(39) Espiau de Lamaëstre, R.; Bernas, H. Significance of Lognormal Nanocrystal Size Distributions. *Phys. Rev. B* **2006**, *73*, 125317.
(40) Sias, U. S.; Moreira, E. C.; Ribeiro, E.; Boudinov, H.; Amaral, L.; Behar, M. Photoluminescence from Si Nanocrystals Induced by High-Temperature Implantation in SiO_2. *J. Appl. Phys.* **2004**, *95*, 5053−5059.
(41) Nikolova, L.; Saint-Jacques, R. G.; Dahmoune, C.; Ross, G. G. Si Nanoparticle Formation in SiO_2 by Si Ion Implantation: Effect of Energy and Fluence on Size Distribution and on SiO_2 Composition. *Surf. Coat. Technol.* **2009**, *203*, 2501−2505.
(42) Bonafos, C.; Colombeau, B.; Altibelli, A.; Carrada, M.; Assayag, G. B.; Garrido, B.; López, M.; Pérez-Rodríguez, A.; Morante, J. R.; Claverie, A. Kinetic Study of Group IV Nanoparticles Ion Beam Synthesized in SiO_2. *Nucl. Instrum. Methods Phys. Res., Sect. B* **2001**, *178*, 17−24.
(43) Garrido Fernandez, B.; López, M.; García, C.; Pérez-Rodriguez, A.; Morante, J. R.; Bonafos, C.; Carrada, M.; Claverie, A. Influence of Average Size and Interface Passivation on the Spectral Emission of Si Nanocrystals Embedded in SiO_2. *J. Appl. Phys.* **2002**, *91*, 798−807.
(44) López, M.; Garrido, B.; Bonafos, C.; Pérez-Rodriguez, A.; Morante, J. R. Optical and Structural Characterization of Si Nanocrystals Ion Beam Synthesized in SiO_2: Correlation Between the Surface Passivation and the Photoluminescence Emission. *Solid-State Electron.* **2001**, *45*, 1495−1504.
(45) Hao, X. J.; Cho, E.-C.; Scardera, G.; Bellet-Amalric, E.; Bellet, D.; Shen, Y. S.; Huang, S.; Huang, Y. D.; Conibeer, G.; Green, M. A. Effects of Phosphorus Doping on Structural and Optical Properties of Silicon Nanocrystals in a SiO_2 Matrix. *Thin Solid Films* **2009**, *517*, 5646−5652.
(46) Gault, B., Moody, M. P., Cairney, J. M., Ringere, S. P., Eds; *Atom Probe Microscopy*; Springer: New York, 2012.
(47) Vaumousse, D.; Cerezo, A.; Warren, P. J. A Procedure for Quantification of Precipitate Microstructures from Three-Dimensional Atom Probe Data. *Ultramicroscopy* **2003**, *95*, 215−221.
(48) Boeisenko, V. E.; Yudin, S. G. Steady-State Solubility of Substitutional Impurities in Silicon. *Phys. Status Solidi* **1987**, *101*, 123−127.
(49) Nomoto, K.; Sugimoto, H.; Breen, A.; Ceguerra, A. V.; Kanno, T.; Ringer, S. P.; Wurfl, I. P.; Conibeer, G.; Fujii, M. Atom Probe Tomography Analysis of Boron and/or Phosphorus Distribution in Doped Silicon Nanocrystals. *J. Phys. Chem. C* **2016**, *120*, 17845−17852.
(50) Crowe, I. F.; Papachristodoulou, N.; Halsall, M. P.; Hylton, N. P.; Hulko, O.; Knights, A. P.; Yang, P.; Gwilliam, R. M.; Shah, M.; Kenyon, A. J. Donor Ionization in Size Controlled Silicon Nanocrystals: The Transition from Defect Passivation to Free Electron Generation. *J. Appl. Phys.* **2013**, *113*, No. 024304.
(51) Guha, S.; Qadri, S. B.; Musket, R. G.; Wall, M. A.; Shimizu-Iwayama, T. Characterization of Si Nanocrystals Grown by Annealing SiO_2 Films with Uniform Concentrations of Implanted Si. *J. Appl. Phys.* **2000**, *88*, 3954−3961.
(52) Normand, P.; Kapetanakis, E.; Dimitrakis, P.; Tsoukalas, D.; Beltsios, K.; Cherkashin, N.; Bonafos, C.; Benassayag, G.; Coffin, H.; Claverie, A.; et al. Effect of Annealing Environment on the Memory Properties of Thin Oxides with Embedded Si Nanocrystals Obtained by Low-Energy Ion-Beam Synthesis. *Appl. Phys. Lett.* **2003**, *83*, 168−170.
(53) Carvalho, A.; Öberg, S.; Barroso, M.; Rayson, M. J.; Briddon, P. P-doping of Si nanoparticles: The Effect of Oxidation. *Phys. Status Solidi* **2012**, *209*, 1847−1850.